Electronic band structure of beryllium oxide

2003 J. Phys.: Condens. Matter 15 3567

(http://iopscience.iop.org/0953-8984/15/21/306)

INSTITUTE OF PHYSICS PUBLISHING JOURNAL OF PHYSICS: CONDENSED MATTER

J. Phys.: Condens. Matter **15** (2003) 3567–3581 PII: S0953-8984(03)56498-0

Electronic band structure of beryllium oxide

V A Sashin[1,5], M A Bolorizadeh[2], A S Kheifets[3] and M J Ford[4]

[1] School of Chemistry, Physics and Earth Science, Flinders University of South Australia, GPO Box 2100, Adelaide SA 5001, Australia
[2] Physics Department, Shahid Bahonar University, Kerman, Iran
[3] Atomic and Molecular Physics Laboratories, Research School of Physical Sciences and Engineering, The Australian National University, Canberra ACT 0200, Australia
[4] Institute for Nanoscale Technology, University of Technology Sydney, PO Box 123, Broadway NSW 2007, Australia

E-mail: Vladimir.Sashin@anu.edu.au

Received 22 November 2002
Published 19 May 2003
Online at stacks.iop.org/JPhysCM/15/3567

Abstract

The energy–momentum resolved valence band structure of beryllium oxide has been measured by electron momentum spectroscopy (EMS). Band dispersions, bandwidths and intervalence bandgap, electron momentum density (EMD) and density of occupied states have been extracted from the EMS data. The experimental results are compared with band structure calculations performed within the full potential linear muffin-tin orbital approximation. Our experimental bandwidths of 2.1 ± 0.2 and 4.8 ± 0.3 eV for the oxygen s and p bands, respectively, are in accord with theoretical predictions, as is the s-band EMD after background subtraction. Contrary to the calculations, however, the measured p-band EMD shows large intensity at the Γ point. The measured full valence bandwidth of 19.4 ± 0.3 eV is at least 1.4 eV larger than the theory. The experiment also finds a significantly higher value for the p-to-s-band EMD ratio in a broad momentum range compared to the theory.

1. Introduction

Beryllium oxide (BeO) has a large (10.6 eV) bandgap and crystallizes into the wurtzite (hexagonal) structure as its stable phase at room temperature (Hazen and Finger 1986). It differs from the other alkaline earth oxides both in its crystal structure and nature of chemical bonding. While other oxides in the group are often considered 'ideal' ionic solids, beryllium oxide shows properties more typical of covalent solids (Joshi *et al* 1999, Sirota and Kuz'mina 1991).

[5] Present address: Atomic and Molecular Physics Laboratories, Research School of Physical Sciences and Engineering, The Australian National University, Canberra ACT 0200, Australia.

The relative simplicity of BeO makes it amenable to high-level computational studies and indeed theoretical reports are well established in the literature (Chang *et al* 1983, Chang and Cohen 1984, Lichanot and Rerat 1993, Kulyabin *et al* 1990, Lichanot *et al* 1992, Xu and Ching 1993). It provides an ideal system for testing the validity of theoretical models. Despite some remaining discrepancies in theoretical predictions, agreement with experimental work continues to improve. The available experimental results, however, provide data integrated over either momentum, in the case of x-ray and photoemission, or binding energy, in the case of Compton scattering, and usually require significant theoretical input for their interpretation. To the authors' knowledge, a complete mapping of the band structure by angle resolved photoemission has not yet been undertaken. In this paper we attempt to bridge this gap, reporting experimental measurements of the full energy and momentum resolved density of states for the valence band of BeO.

The first measurements of the valence band electronic structure were carried out by O'Bryan and Skinner (1940), using soft x-ray spectroscopy. They obtained rather large values of 23 and 12 eV for the 2p and 2s valence bandwidths, respectively. Lukirskii and Brytov (1964) and Fomichev (1971) measured emission and absorption spectra in BeO, thereby allowing them to construct the complete energy-level diagram. They found a much smaller width for the 2p valence band (8.8 eV (Lukirskii and Brytov 1964) and 10.3 eV (Fomichev 1971), respectively). Hamrin *et al* (1970) performed ESCA measurements on the isoelectronic series LiF, BeO, BN and graphite, and produced a reliable energy mapping of the core lines and valence bands. Optical reflectance measurements by Roessler *et al* (1969) and the electron energy loss (EEL) measurements of Gründler *et al* (1978) have also had a significant input to our understanding of the electronic properties of BeO. The first attempts to measure Compton profiles in BeO were made by Fukamachi and Hosoya (1970) and Weiss (1970). A recent experimental work from Joshi *et al* (1999) shows very good agreement with the calculations of Lichanot *et al* (1992), using the Hartree–Fock linear combination of atomic orbitals (HF LCAO) approach.

In the following sections we report measurements of the electronic structure of BeO using electron momentum spectroscopy (EMS). EMS measures the probability that an electron in a target has a certain binding energy and momentum (McCarthy and Weigold 1988). In our experiment an energetic incoming electron with well known energy and momentum scatters from an electron of the target. At a large energy transfer the target electron is ejected. The scattered and ejected electrons are subsequently detected in coincidence and their momenta and energies are determined. Using the conservation laws of energy and momentum the binding energy and real momentum (not crystal momentum) of the target electron just before the collision are then obtained. A large number of these coincidence events give a distribution of the target electrons over energy–momentum space, i.e. energy–momentum resolved density or spectral momentum density of the material. Its integration over binding energy or momentum gives, respectively, electron momentum density (EMD) as a function of electron momentum or occupied density of states (DOS) as a function of electron binding energy. By fitting quasi-particle peak positions one can also determine the dispersion relationship for the target electrons. We compare the experimental results, in terms of dispersion, EMD and DOS, to calculations based on the density functional theory in the local density approximation (DFT-LDA) implemented in the full potential linear muffin-tin orbital (FP-LMTO) method.

2. Experimental techniques

We give here only an outline of our EMS spectrometer. A detailed description can be found elsewhere (Storer *et al* 1994, Canney *et al* 1997). Operation of the spectrometer is based on the

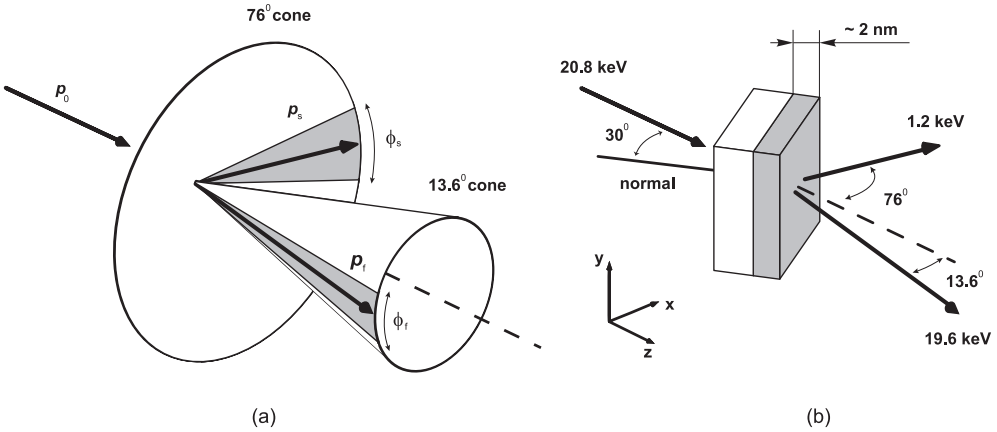

Figure 1. Layout of (a) the scattering geometry, and (b) target orientation with respect to incident and two outgoing electrons. Shaded sectors of the cones in (a) designate the angular acceptance of the analysers. The shaded layer in (b) represents the portion of the target that contributes most to the measured spectral momentum density.

so-called (e, 2e) reaction (McCarthy and Weigold 1988, 1991, Coplan *et al* 1994)—a process where an incident electron ionizes a target with subsequent detection of the two outgoing electrons. If the energy of the incident electron is sufficiently high and substantial momentum is transferred to the target electron then the collision can be regarded as a 'billiard-ball'-like interaction between the incident and target electrons (the plane-wave impulse approximation, or PWIA). Knowing the complete kinematics of the incident and two outgoing electrons, the kinematical parameters of the target electron immediately before collision can be deduced. In the PWIA the binding energy ε and momentum $\boldsymbol{q}$ of the target electron are determined by conservation of energy and momentum:

$$\begin{aligned} \varepsilon &= E_0 - E_s - E_f \\ \boldsymbol{q} &= \boldsymbol{p}_s + \boldsymbol{p}_f - \boldsymbol{p}_0, \end{aligned} \tag{1}$$

where $(E_0, \boldsymbol{p}_0)$, $(E_s, \boldsymbol{p}_s)$ and $(E_f, \boldsymbol{p}_f)$ refer to the energies and momenta of the incident and two outgoing electrons, respectively. Subscripts s and f stand for slow and fast outgoing electrons. The overall (e, 2e) cross section is proportional to the absolute square of the momentum space wavefunction of the target electron (McCarthy and Weigold 1991), hence the name EMS.

Figure 1(a) shows the scattering geometry of our spectrometer. It exploits highly asymmetric non-coplanar kinematics. The incident and two outgoing electrons have nominal energies of 20.8, 19.6 and 1.2 keV, respectively. The outgoing electrons are detected in coincidence by two electrostatic energy analysers at polar angles of 13.6° and 76° relative to the incident beam, and over a range of ±6° and ±10° azimuthal angles, respectively. This gives an overall detectable momentum range of about ±2.5 atomic units (au) along the y-axis. The overall energy and momentum resolutions of the spectrometer are 1 eV and 0.15 au, respectively. The escape depth of the 1.2 keV electrons is only about 2 nm so that the spectrometer is relatively surface sensitive. This feature makes it possible to perform measurements from targets prepared by evaporation onto a thin substrate. The shading in figure 1(b) designates the surface layer from which most electronic structure information comes. (e, 2e) events taking place deeper within the target (non-shaded area) contribute mainly to a background intensity.

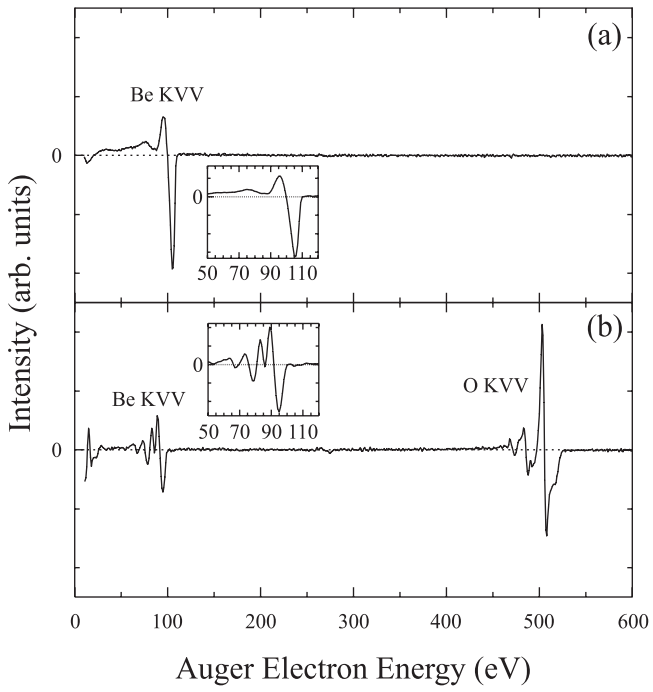

Figure 2. Differential Auger spectrum of the target surface, (a) immediately after deposition of the beryllium layer and (b) after oxidation. The insets show a magnified view of the Be KVV line.

Preparation of the BeO targets consists of two stages. During the first, pure (99.5%) beryllium is evaporated onto an am-C substrate (3 nm thick) from a tungsten boat by resistive heating. A series of different Be coverages, ranging from 1 to 10 nm, has been tried. It was found that targets with 3 nm coverage gave the optimum (e, 2e) signal. The beryllium surface was monitored by Auger electron spectroscopy. A typical differential Auger spectrum of a freshly prepared beryllium target is presented in figure 2(a). It shows the Be KVV line at 105 eV, and two small satellites at approximately 86 and 67 eV. These satellites are shifted from the main peak by multiples of about 19 eV, which is the bulk plasmon energy loss in metallic beryllium. Thus they are considered to be due to first and second order plasmon losses experienced by the Auger electrons (Sashin *et al* 2001, Suleman and Pattinson 1971, Zehner *et al* 1973). The fact that no other peaks are visible in this spectrum implies a clean and fully covered surface.

For the second stage of preparation (post-oxidation), the Be layer was heated to about 600 °C in an oxygen atmosphere of 3×10^{-7} Torr for about 20 min (a dose of 360 Langmuirs). According to Fowler *et al* (1983) who investigated the oxidation kinetics of the Be(0001) surface under UHV conditions, one could reasonably expect formation of at least 12 oxide monolayers (approximately 3 nm) under these conditions. Thus, a 3 nm beryllium layer will be completely oxidized. The structure of the prepared BeO targets is expected to be polycrystalline (Gruner and Mollenstedt 1972).

A typical differential Auger spectrum of the oxide surface is shown in figure 2(b). It compares favourably with previously reported spectra of oxidized beryllium (LeJeune and Dixon 1972). The appearance of the O KVV line at about 512 eV, and a drastic change in the position and shape of the Be KVV line, are indicative of the chemical transformation of

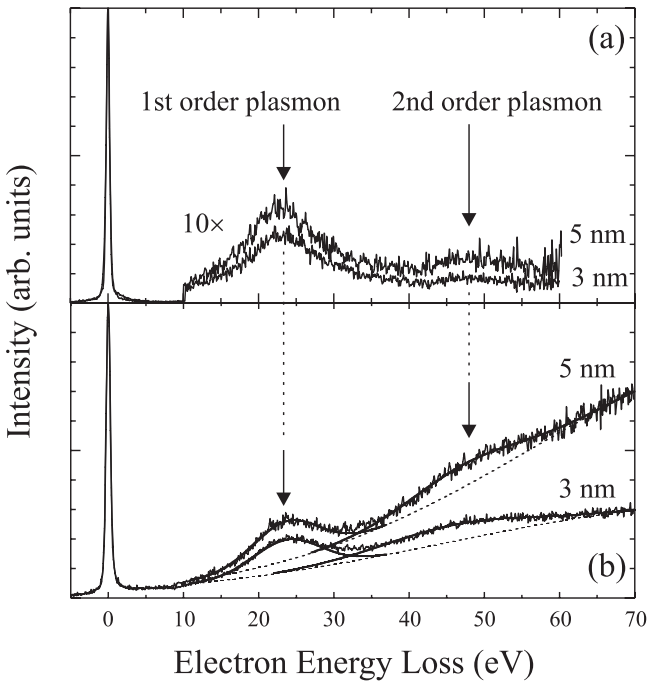

Figure 3. EEL spectra for 3 and 5 nm BeO targets: (a) 19.6 keV electrons and (b) 1.2 keV electrons. In (b) the solid curves are the result of least squares fits to the first and second order bulk plasmon losses in beryllium oxide superimposed on a smooth background (dashed curves).

metallic beryllium to the oxide species. The Be KVV line in BeO is shifted to lower energy by about 10 eV (Fortner and Musket 1971). A series of satellites, at about 86, 78 and 68 eV, accompanies the 95 eV Be KVV peak. These energies agree well with the values obtained by both (Zehner *et al* 1973) and (Fowler and Blakely 1982). The main line at 95 eV and the satellite at 86 eV originate from the 1s2p2p transitions involving one 1s electron of the K-shell and two 2p electrons from the top and bottom region of the p band, respectively (LeJeune and Dixon 1972). The 78 eV satellite is probably due to the 1s2p2s transition involving one 2s electron from the s band. The last satellite peak at 68 eV, separated from the main line by 27 eV, is thought to be due to energy loss in the BeO layer. No sign of surface contamination is observed in this spectrum.

Figures 3(a) and (b) show our transmission EEL spectra for 19.6 and 1.2 keV electrons, respectively, incident on two different BeO targets. One can clearly see an intense, broad structure that is centred at about 24 eV, and a weaker structure that is centred at around 50 eV. These are the first and second order plasmon energy losses, respectively. From our separate EEL measurements on an am-C substrate we know that there is a bulk plasmon at 23 eV with halfwidth of 17 eV. Previous measurements of the bulk plasmon in BeO give energies ranging from 21 eV (Jenkins *et al* 1973) to 28 eV (Watanabe 1954, Bashenov *et al* 1974). Hence, plasmon losses due to the am-C substrate and BeO overlayer will overlap in the spectra of figure 3.

In an attempt to quantify the EEL peaks for BeO, least squares fits to the first and second order plasmon losses in figure 3(b) have been performed. The fitting functions are two Gaussians to represent the first and second order BeO plasmon energy losses and a Gaussian-

like background to represent all other inelastic processes, including the am-C plasmon loss. The fits give values of 23.7 ± 0.2 and 46.5 ± 0.5 eV for the energies of the first and second order plasmons in BeO, and 10.5 ± 0.5 and 20 ± 3 eV for their halfwidths, respectively. Using the free electron model, with six valence electrons per BeO molecule, we calculate a plasmon energy of about 24.5 eV. This value is remarkably close to that obtained experimentally, particularly in view of the simplicity of this model. The present EEL values for BeO are also within the range reported in previous measurements (Jenkins *et al* 1973, Watanabe 1954, Bashenov *et al* 1974). There are no explicit data in the literature for the halfwidth of this energy loss feature, but a typical width is about 5 eV (Roessler *et al* 1969), in qualitative agreement with our data.

One can estimate the thickness of the oxidized BeO layer, in our targets, from the intensities of the first and second order plasmons in the 1.2 keV EEL spectra. The probability of producing n bulk plasmons in a target of thickness x is governed by a Poisson distribution:

$$p_n(x) = (1/n!)(x/\lambda)^n \exp(-x/\lambda), \tag{2}$$

where λ is the mean free path for plasmon excitation. From the ratios of the peak intensities the average value of (x/λ) is found to be equal to 2.0 ± 0.2 for targets of either thickness. In other words, whether 3 or 5 nm of Be are deposited onto the substrate, the thickness of the BeO layer that forms during the oxidation process is approximately the same. There are no experimental data for λ in BeO for 1.2 keV electrons in the literature. Using the formula proposed by Penn (1976), we estimate the inelastic mean free path for these electrons to be 1.65 ± 0.17 nm. This value can then be taken as the lower limit for the mean free path for plasmon excitation, λ. Since the 1.2 keV electrons traverse the target at an angle of 45° relative to the surface normal (see figure 1(b)) we obtain a value for the minimal thickness of the BeO layer of 2.3 ± 0.2 nm. This value compares favourably with that calculated from the data of Fowler *et al* (1983) for the oxidation dynamics of beryllium. One can reiterate our previous conclusion that we have complete oxidation for the 3 nm BeO target, and partial oxidation in the case of the 5 nm BeO target. The absence of any energy loss structure at about 19 eV due to a buried Be layer in our EEL spectrum for the latter target could be understood in terms of a reduction of the bulk plasmon probability in extremely thin layers (Raether 1967).

3. FP-LMTO calculation

The band structure and EMD were calculated using the FP-LMTO method with lattice parameters from Wyckoff (1963) of 2.698 and 4.380 Å. There are four non-equivalent atomic positions in the unit cell. The beryllium atoms occupy the $(0, 0, 0)$ and $(1/3, 2/3, 1/2)$ positions, whereas the oxygen atoms are found at $(0, 0, u)$ and $(1/3, 2/3, u + 1/2)$, where $u = 0.378$. Four equal size muffin-tin spheres were placed at these atomic positions so that the Be sphere at $(0, 0, 0)$ was touching the oxygen spheres at the neighbouring sites.

The calculated energy bands and individual EMDs of BeO along several high-symmetry directions of the lattice are shown in figure 4. In the top panel the energy bands, or crystalline orbitals, are plotted as a function of the high symmetry points of the reciprocal crystal lattice in the reduced zone scheme. The unit cell of the reciprocal lattice (first Brillouin zone) showing the location of these symmetry points is also shown in the figure 4. The bottom panels show the probability distribution of the electrons plotted as a function of electron momentum (the EMD).

The two lowest valence bands (numbered 1 and 2, and collectively named the s band) are derived from the 2s orbitals of the oxygen ion, while the cluster of six upper bands, numbered from 3 to 8 (the p bands), is derived predominantly from the oxygen 2p orbitals. Note that two of the six p valence bands in the ΓA direction are degenerate.

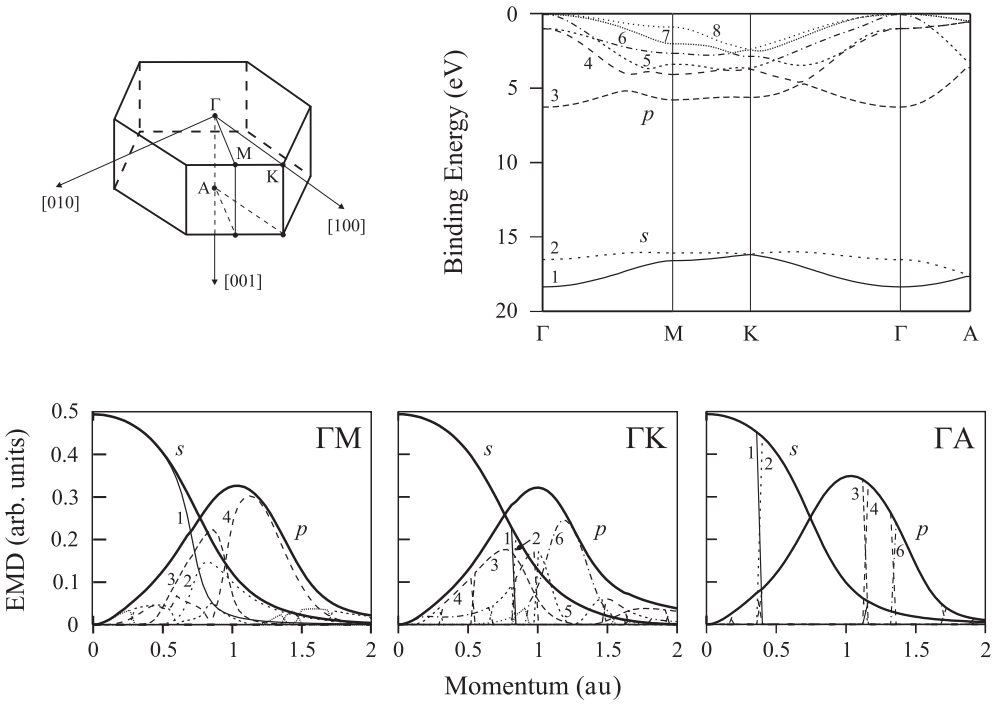

Figure 4. Energy bands and EMDs for BeO, as calculated within the FP-LMTO approximation along several high symmetry directions. The first Brillouin zone is also shown. Energy bands are represented in the reduced zone scheme with corresponding EMDs shown by the same line style. The energy bands and some EMD curves are numbered to facilitate their correspondence. The summed EMD of the s and p valence bands is shown in each case by thick solid curves.

4. Results and discussion

4.1. Band intensities

The measured energy resolved momentum density of the BeO valence band is shown in figure 5(a). The binding energy is relative to the vacuum level of the spectrometer. The picture is typical for the valence band structure of an ionic solid, showing two structures separated by an energy gap. It is convenient to label them as an s and a p band, referring to the lower and upper valence bands, respectively. The p band ranges from about 10 to 15 eV, while the s band is located at around 28 eV with a spread in binding energy of about 2 eV. The corresponding momentum ranges are 1.3 au for the p band and 0.7 au for the s band. There is also a very faint parabolic structure, dispersing from about 5 to 19 eV, visible in figure 5(a). This structure originates from the am-C substrate, as its energy-width is consistent with previous data (Vos *et al* 1995). Additional intensity in figure 5(a), especially noticeable between the branches of the bands and below the s band, is the result of multiple scattering of (e, 2e) electrons in the target.

The result of the FP-LMTO band structure calculation is presented in figure 5(b). The density has been spherically averaged over the irreducible wedge of the Brillouin zone (Kheifets and Cai 1995) to account for the polycrystalline nature of the measured target, and convoluted with Gaussians (halfwidths of 1 eV and 0.15 au) to account for the experimental resolutions. The energy scale in the calculations is shifted by approximately 11 eV to match the energy of

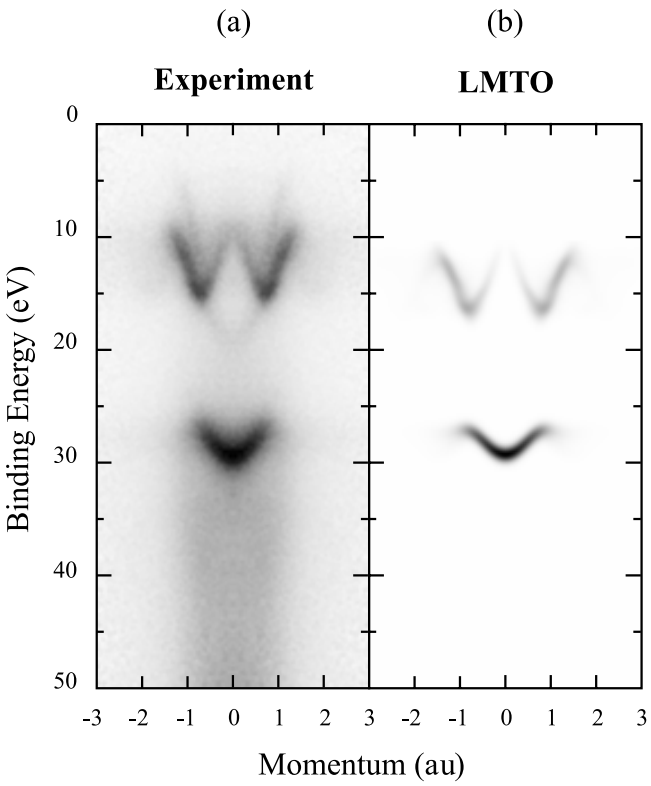

Figure 5. Energy–momentum resolved densities, (a) measured by EMS and (b) calculated within the FP-LMTO approximation. Electron density is depicted on a linear grey scale: a darker colour corresponds to higher density.

the bottom of the s band in the experiment. This energy shift reflects the fact that the measured energies are relative to the spectrometer vacuum level, whereas the calculations are relative to the valence band maximum. There is qualitative agreement between theory and experiment in terms of the shape of both bands. However, a careful comparison of figures 5(a) and (b) shows that there are significant differences in the relative intensity of the p and s bands and the magnitude of the intervalence bandgap.

Figure 6 shows binding energy profiles extracted from figures 5(a) and (b) by taking vertical slices integrated over 0.15 au momentum ranges. The positive and negative momentum regions have been added to improve statistics. A smooth background has been subtracted from the experimental data using a least squares fitting procedure. The fitted function representing this background is the sum of a second order polynomial and a Gaussian to account for first order plasmon excitation from the p band. The faint parabola between 5 and 19 eV has also been removed by assuming it originates from am-C. Experimental and calculated intensities and energies have been normalized at the s-band peak in the 0 au momentum interval.

Considering first the experimental data, it is apparent that the s band disperses towards smaller energy as the momentum increases. Conversely, the p band initially disperses towards higher energy as the momentum increases, until a momentum of about 0.75 au is reached, after which it disperses toward smaller energy. The shape of the s-band peak is Gaussian-like whereas that of the p band is more complex. This difference in the profile shapes may be caused, at least in part, by elastic scattering in the target.

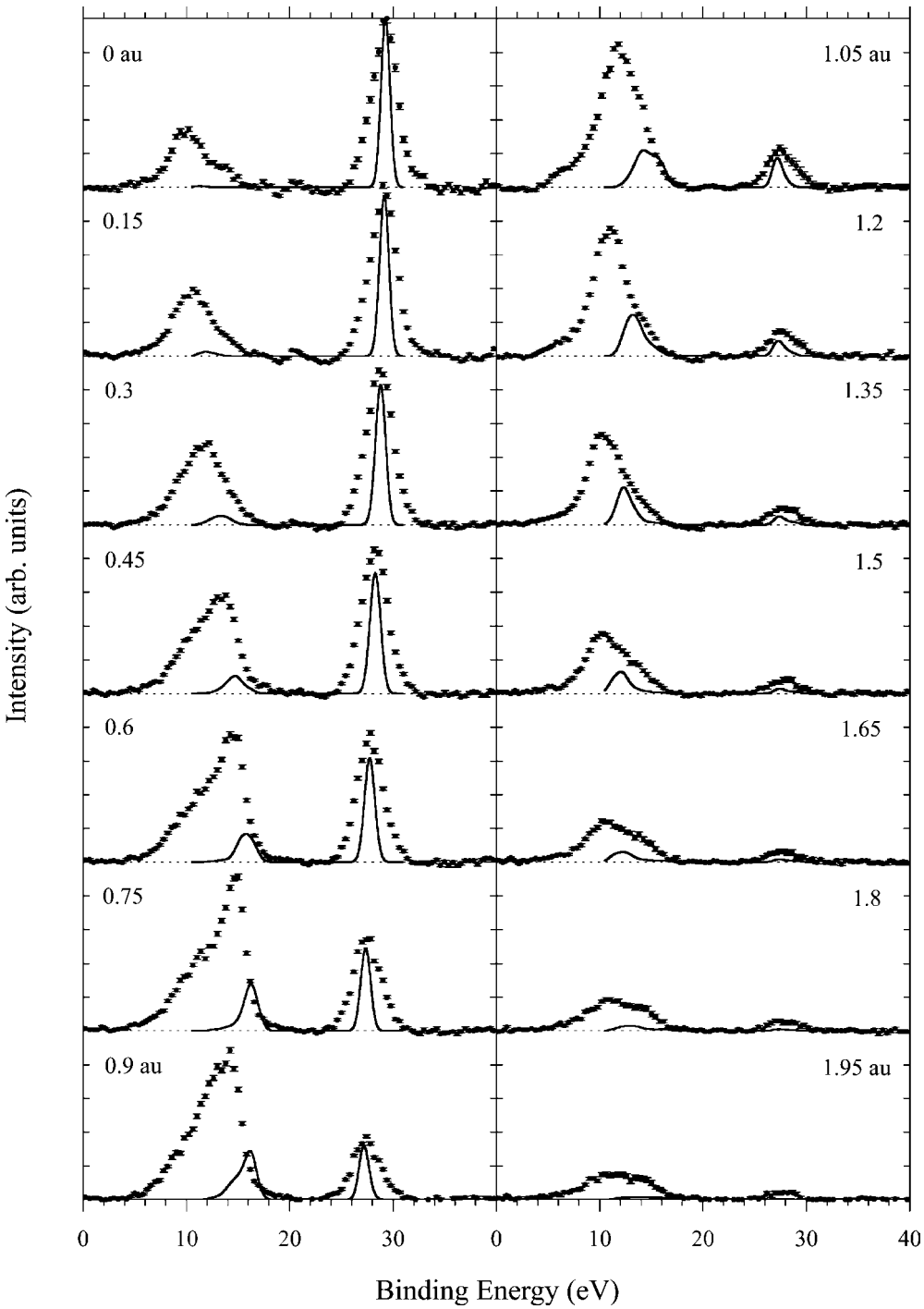

Figure 6. Comparison of binding energy profiles from the experiment (points with error bars) and convoluted LMTO calculation (solid curve). The profiles are obtained from figure 5 by taking vertical slices integrated over 0.15 au momentum width intervals with the midpoint momentum shown in each panel. A smooth background due to multiple scattering is subtracted from the experimental data.

The momentum behaviour of the experimental and theoretical intensities for the s band is quite similar over the whole momentum range. However, the experimental peaks are significantly broader (FWHM is about 3 eV) compared to those from the LMTO (about 1 eV). This extra broadening can be, at least partially, attributed to multiple scattering in the target.

There are a number of discrepancies between experiment and theory for the p band. Firstly, theory predicts nearly zero intensity at 0 au whereas the experiment shows a broad peak with an intensity that is about 40% of the maximum value that occurs at about 0.75 au momentum. Secondly, the widths of the experimental peaks (about 5.5 eV) are much broader than those from the convoluted LMTO calculation (about 3 eV). Elastic scattering of the (e, 2e) electrons leading to a 'smearing' of intensity along the momentum axis may contribute to both these discrepancies. The same mechanism can produce intensity at high momentum values. In the 1.95 au interval of figure 6, for example, the theoretical intensity of the p band is close to zero, while the experiment exhibits a broad peak with intensity about 20% of the maximum amplitude. Experiment and theory also differ in the intensity ratio of the p band to s band, being much larger in the measurement compared to the theoretical prediction. As we have seen above, multiple scattering tends to smear intensity along the momentum (elastic scattering) or energy (inelastic scattering) axis and is unlikely to redistribute intensity between the two bands to such a significant value as seen in the intensity ratio. The final discrepancy to note is the magnitude of the intervalence bandgap, which is about 1.5 eV larger in the experiment compared to that calculated by theory.

Further analysis of the data has been undertaken by least squares fitting of binding energy profiles similar to figure 6. The data are integrated over 0.05 au momentum intervals and the peak maxima fitted with a Gaussian function. The intensity, width and energy position of the Gaussian are determined by the least squares fit. From this fit we can determine the band dispersion, which, together with the calculated EMD and DOS, is presented in the following sections.

4.2. Lower valence band

The oxygen s-band dispersion and EMD extracted from the experimental and theoretical binding energy profiles are shown in figure 7. Errors bars on the experimental data reflect the error in the fitting procedure. The relatively small dispersion is indicative of small overlap between 2s orbitals situated on neighbouring ions. There is very good agreement between the experiment and the LMTO dispersion up to about 0.9 au in momentum. Beyond this point it is difficult to fit the experimental data reliably because of the small intensity of the s band.

Estimates of the occupied bandwidth can be calculated from these dispersion relationships by taking the energy difference between the band bottom and top. Bandwidths of 2.1 ± 0.2 and 2.12 eV, for the experiment and convoluted LMTO calculation, respectively, as extracted from figure 7, are also in good agreement. These bandwidths have been extracted from spherically averaged and convoluted data and so care must be taken when comparing them to other work, either theoretical or experimental. The s bandwidth can also be deduced from the calculated DOS or equivalently from the band extrema in figure 4. In this case the value is 2.3 eV which also agrees, to within error, with our experimental value and is only slightly larger than the theoretical value from figure 7. The s bandwidth is not greatly affected by spherical averaging and convolution.

The experimental and LMTO EMDs agree to within the experimental uncertainty, up to about 1.05 au in momentum. Beyond this point the experimental EMD is larger, possibly due to the effects of elastic scattering.

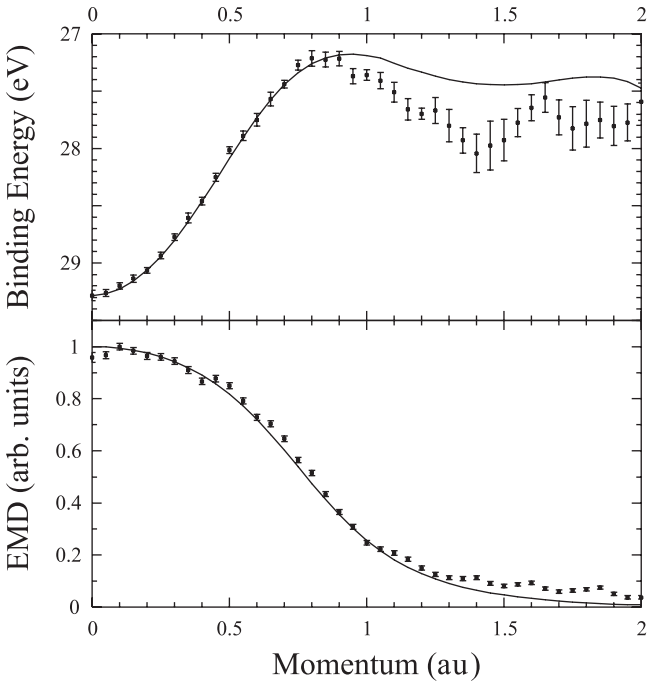

Figure 7. Comparison of s-band dispersions (upper panel) and EMDs (lower panel), as extracted from binding energy profiles similar to those presented in figure 6, but with a finer (0.05 au) binding. Points with error bars are the experiment, while the solid curve is the convoluted LMTO calculation. In the lower panel the experimental and LMTO EMDs are normalized to unity.

4.3. Upper valence band

The upper valence band, or p band, is derived predominantly from the 2p orbitals of the oxygen anion, with a relatively small contribution from the orbitals associated with the metallic cation. Overlap of neighbouring O 2p orbitals is larger compared to that of the O 2s orbitals, leading to a significantly larger bandwidth.

The p-band dispersion curves and EMDs obtained by least squares fits to the binding energy profiles are shown in figures 8(a) and (b). Experimental and calculated binding energies have been normalized at the p-band minimum in figure 8 to account for the different zero-energy points of the measurement and LMTO calculation. The occupied DOS, as a function of binding energy, in the p band has also been extracted from the experimental and theoretical momentum profiles (horizontal slices through figure 5 integrated over 0.5 and 0.2 eV intervals, respectively). The results are shown in figure 8(c).

The overall shapes of the experimental and theoretical dispersion curves in figure 8(a) are reasonably similar. Beyond about 2 au the p-band intensities are relatively small and hence the dispersion curve cannot be determined very reliably. The experimental dispersion points rise earlier from the bottom of the band (around 0.7 au up to 1.4 au momentum) compared with the calculation. The band intensity is at a maximum over this region so the dispersion curve can be obtained reliably with minimal contribution from multiple scattering. Possible causes include a small misalignment of the spectrometer or a limitation of the DFT-LDA approach in describing the electron correlations.

The experimental p bandwidth is 4.8 ± 0.3 eV, which compares well with the value of 5.01 eV from the convoluted LMTO data. The minimum of the p band is taken to be at about

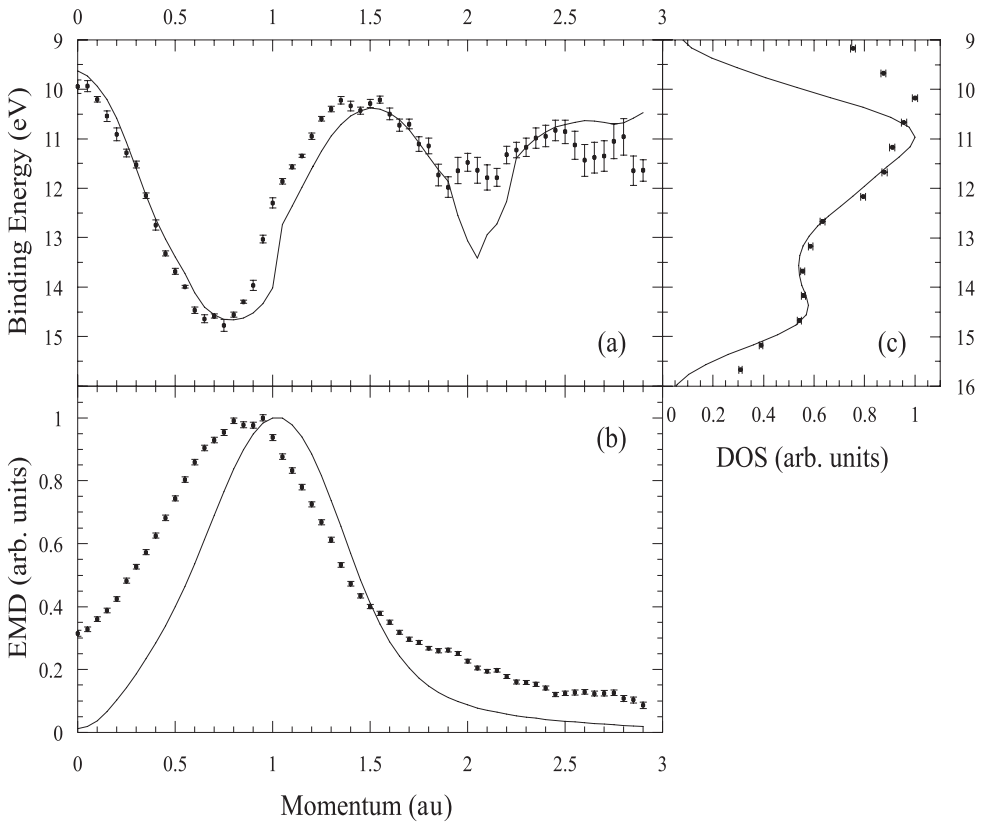

Figure 8. Comparison of the experiment and theory in regard to (a) p-band dispersions, (b) EMDs and (c) occupied DOS. Full points with error bars and solid curves are derived from the experiment and convoluted LMTO calculation, respectively. Dispersions (a) and EMDs (b) are calculated from binding energy profiles similar to those presented in figure 6, but with a finer (0.05 au) binning. The DOS data are derived from momentum profiles obtained from figure 5 by integration over 0.5 eV (experiment) and 0.2 eV (LMTO) binding energy width intervals. In (b) and (c) the experiment and LMTO data are both normalized to unity.

0.8 au of momentum, and the maximum is considered to be at zero momentum. As was the case for the s band, these values are deduced from spherically averaged and convoluted data. The value extracted from the calculated DOS or band extrema in figure 4 is 6.275 eV. For the p band, spherical averaging and convolution reduce the bandwidth by over 1 eV. Previous values for the bandwidth obtained from x-ray and photoemission measurements range from 6.8 eV (Kulyabin *et al* 1990) to 10.3 eV (Fomichev 1971). These values are taken from the width of the measured DOS. Differences in these values may possibly be ascribed to how the width is determined from the data or experimental resolution. These values cannot be compared directly with our value; nonetheless, they are all clearly larger than our calculated value extracted from the DOS or band extrema. Our previous calculations (Sashin *et al* 2000) using the linear combination of atomic orbitals (LCAO) approximation with LDA, GGA and hybrid DFT functionals give results ranging from 6.36 to 6.88 eV, in better agreement with the x-ray emission measurement reported by Kulyabin *et al* (1990).

The experimental EMD differs significantly from the LMTO result shown in figure 8(b). The experiment shows a relatively large value at zero momentum, while the theoretical

prediction is about an order of magnitude smaller. Elastic scattering of (e, 2e) electrons in the target will contribute to the density at 0 au; however, it is difficult to see that this mechanism could cause such a drastic change in the intensity, creating about 30% of the maximum intensity where the theory predicts virtually no intensity. The maximum in the experimental EMD is shifted to lower momentum, by about 0.2 au, compared to the maximum position of the LMTO calculation. This mirrors the shift difference in the minimum of the dispersion curve.

The experimental and theoretical DOSs show good agreement in the energy range from 11 to 15 eV. The experimental DOS is broader, presumably due to the experimental binding energy peaks being much wider than the convoluted LMTO calculation (see figure 6). A two-peak structure is clearly visible in both data sets. The positions of the respective peak maxima are at about 14.5 and 11 eV for the calculation and 14.5 and 10.5 eV for the experiment. The energy separation between the two peaks is in reasonable agreement with the value of 3.4 eV obtained by Hamrin *et al* (1970). In addition, the intensity ratios of the two peaks, about 0.6 from the present DOS and 0.7 from figure 3 of Hamrin *et al* (1970) agree quite well.

4.4. Full valence bandwidth

It is clear from figure 5 that the full valence bandwidth, or intervalence bandgap, is larger in the experiment than in the calculation. The values for the full valence bandwidths extracted from the dispersion curves are 19.4 ± 0.3 and 18.02 eV for the experiment and calculation, respectively. Previous experimental values are about 20.5 and 21.3 eV from the x-ray emission and absorption measurements of Lukirskii and Brytov (1964) and Fomichev (1971), respectively, and about 21 eV from the photoemission measurements of Hamrin *et al* (1970). Our previous LCAO calculations range from 18.69 eV for gradient corrected DFT to 20.13 eV for the B3-PW hybrid functional.

4.5. Intensity ratio

As we mentioned previously, there is a noticeable difference between the measured and calculated ratio of p-to-s-band intensity, with the experiment showing a higher relative intensity in the p band. To illustrate this point quantitatively we have calculated the p-to-s-band EMD ratio. The result is plotted in figure 9. In addition to the difference at zero momentum mentioned previously, the experimental ratio is systematically larger throughout the first 1.3 au momentum interval. The LMTO ratio slowly increases from 0 to 1 at about 0.75 au followed by a nearly linear rise to a value of 5.5 at about 1.4 au. Thereafter, the LMTO ratio is essentially constant up to a momentum of 1.75 au, where there is a second rise. The experimental ratio exhibits qualitatively similar behaviour, although this ratio is only reliable for momentum between approximately 0.3 and 1 au; above this point multiple scattering, particularly for the s band, plays a crucial role.

There is no doubt that multiple scattering, to some degree, affects the experimental EMD ratio. This change is not, however, expected to be very significant in the middle of the 0–1 au momentum interval, where the intensities of both bands are relatively high. Consequently, the observed discrepancy in figure 9 between experiment and theory is not simply an artefact of multiple-scattering processes, but could be a manifestation of the many-electron correlations, which are not included properly in the present DFT-LDA calculation.

5. Conclusion

In this paper we have presented the full energy and momentum resolved electronic structure of the valence band in beryllium oxide measured using EMS. We have also compared

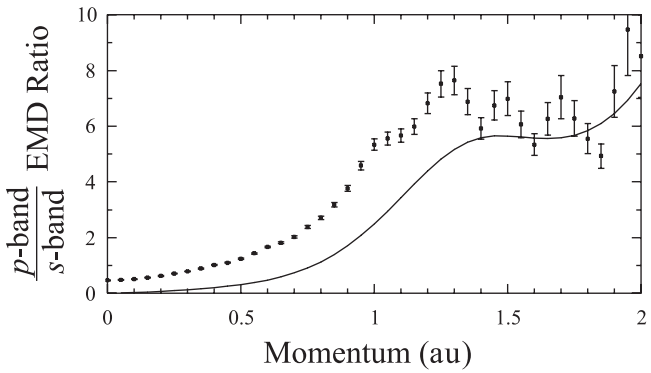

Figure 9. Momentum dependence of the p-to-s-band EMD ratio, as extracted from binding energy profiles of the experiment (points with error bars) and the convoluted LMTO calculation (solid line).

our experimental results to *ab initio* band structures calculated within the FP-LMTO approximation.

Our theoretical calculation gives a reasonable overall prediction of the experimental dispersions in both the upper O 2p and lower O 2s valence bands, except for the 0.8–1.3 au momentum region in the p band where the experimental dispersion curve is 0.1 au narrower in momentum. This result is mirrored by the positions of maxima of the electron momentum densities. Possible explanations involve such assumptions as a small misalignment of the spectrometer scattering geometry or some inadequacy in describing the electron correlations by the DFT-LDA approach. Experimental and theoretical bandwidths for both bands agree within the experimental uncertainty after including the finite energy and momentum resolution of the spectrometer and spherical averaging of the calculation to account for the polycrystalline nature of the sample. The full valence bandwidth from the measurement of 19.4 ± 0.3 eV is about 1.4 eV larger than that predicted by the LMTO calculation.

The experimental EMD for the s-band agrees very well with the theory while there are considerable deviations for the p band. First of all, at the Γ point the theoretical p-band EMD has virtually zero momentum density, as conventional wisdom would suggest for a band derived mainly from p-like orbitals. However, the density observed experimentally is very considerable. Multiple scattering must clearly play a role in this difference. Secondly, the ratio of p-to-s-band intensity is also considerably larger in the experiment when compared with the calculation. This discrepancy exists across a wide momentum range and cannot easily be explained solely on the grounds of multiple scattering. It could be a manifestation of the many-electron correlations not accounted for properly by the DFT-LDA calculation.

In the above analysis it must be remembered, however, that, strictly speaking, DFT methods do not yield true single-particle energies even if the exact density functionals are known.

The experimental data presented in this paper can provide a thorough test of theoretical models. There are, however, a number of issues, which we intend to refine in future work. Multiple-scattering effects will be included by extending our Monte Carlo technique to materials containing more than one atom type. Calculations can be performed that account for the fact that the target is a relatively thin film. It is also worthwhile to compare these experimental results with, for example, many-body Green function calculations to assess the importance of electron correlations.

Acknowledgments

This work was supported by grants from the Australian Research Council and Flinders University.

References

Bashenov V K, Alarashi R A and Foigel M G 1974 *Phys. Status Solidi* b **63** 403
Canney S A, Brunger M J, McCarthy I E, Storer P J, Utteridge S, Vos M and Weigold E 1997 *J. Electron Spectrosc. Relat. Phenom.* **83** 65
Chang K J and Cohen M L 1984 *Solid State Commun.* **50** 487
Chang K J, Froyen S and Cohen M L 1983 *J. Phys. C: Solid State Phys.* **16** 3475–80
Coplan M A, Moore J H and Doering J P 1994 *Rev. Mod. Phys.* **66** 985–1013
Fomichev V A 1971 *Sov. Phys.–Solid State* **13** 754–6
Fortner R J and Musket R G 1971 *Surf. Sci.* **28** 339
Fowler D E and Blakely J M 1982 *J. Vac. Sci. Technol.* **20** 930
Fowler D E, Gyulai J and Palmstrom C 1983 *J. Vac. Sci. Technol.* A **1** 1021
Fukamachi T and Hosoya S 1970 *J. Phys. Soc. Japan* **28** 161
Gründler R, Breuer K and Tews W 1978 *Phys. Status Solidi* b **86** 329
Gruner H and Mollenstedt G 1972 *Thin Solid Films* **14** 43
Hamrin K, Johansson G, Gelius U, Nordling C and Siegbahn K 1970 *Phys. Scr.* **1** 277
Hazen R M and Finger L W 1986 *J. Appl. Phys.* **59** 3728–33
Jenkins L H, Zehner D M and Chung M F 1973 *Surf. Sci.* **38** 327
Joshi K B, Jain R, Pandya R K, Ahuja B L and Sharma B K 1999 *J. Chem. Phys.* **111** 163
Kheifets A S and Cai Y Q 1995 *J. Phys.: Condens. Matter* **7** 1821–33
Kulyabin B E, Lobach V A and Kruzhalov A V 1990 *Sov. Phys.–Solid State* **32** 2138
LeJeune E J and Dixon R D 1972 *J. Appl. Phys.* **43** 1998
Lichanot A, Chaillet M, Larrieu C, Dovesi R and Pisani C 1992 *Chem. Phys.* **164** 383–94
Lichanot A and Rerat M 1993 *Chem. Phys. Lett.* **211** 249
Lukirskii A P and Brytov I A 1964 *Sov. Phys.–Solid State* **6** 33–40
McCarthy I E and Weigold E 1988 *Rep. Prog. Phys.* **51** 299–393
McCarthy I E and Weigold E 1991 *Rep. Prog. Phys.* **54** 789
O'Bryan H M and Skinner H W B 1940 *Proc. R. Soc.* A **176** 229
Penn D R 1976 *J. Electron Spectrosc. Relat. Phenom.* **9** 29
Raether H 1967 *Surf. Sci.* **8** 233–46
Roessler D M, Walker W C and Loh E 1969 *J. Phys. Chem. Solids* **30** 157–67
Sashin V A, Bolorizadeh M, Kheifets A S and Ford M J 2001 *J. Phys.: Condens. Matter* **13** 4203
Sashin V A, Dorsett H E, Bolorizadeh M and Ford M J 2000 *J. Chem. Phys.* **113** 8175
Sirota N N and Kuz'mina A M 1991 *Sov. Phys.–Dokl.* **36** 245
Storer P, Caprari R S, Clark S A C, Vos M and Weigold E 1994 *Rev. Sci. Instrum.* **65** 2214
Suleman M and Pattinson E B 1971 *J. Phys. F: Met. Phys.* **1** L24
Vos M, Storer P, Cai Y Q, McCarthy I E and Weigold E 1995 *Phys. Rev.* B **51** 1866–73
Watanabe H 1954 *J. Phys. Soc. Japan* **9** 920
Weiss R J 1970 *Phil. Mag.* **21** 1169
Wyckoff R W G 1963 *Crystal Structures* vol 1 (New York: Interscience)
Xu Y N and Ching W Y 1993 *Phys. Rev.* B **48** 4335
Zehner D M, Barbulesco N and Jenkins L H 1973 *Surf. Sci.* **34** 385